A high temporal resolution data set of ERS scatterometer radar backscatter for research in Arctic and sub-Arctic regions

Yongwei Sheng, Laurence C. Smith, Karen E. Frey, and Douglas E. Alsdorf
Department of Geography, University of California, Los Angeles, 1255 Bunche Hall, Box 951524, Los Angeles, CA 90095-1524, USA

Received June 2001

ABSTRACT. Radar backscatter in Arctic and sub-Arctic regions is temporally dynamic and reflects changes in sea ice, glacier facies, soil thaw state, vegetation cover, and moisture content. Wind scatterometers on the ERS-1 and ERS-2 satellites have amassed a global archive of C-band radar backscatter data since 1991. This paper derives three high temporal resolution data products from this archive that are designed to facilitate scatterometer research in high-latitude environments. Radar backscatter data have a grid spacing of 25 km and are mapped northwards from 60°N latitude over intervals of one, three, and seven days for the period 1991–2000. Data are corrected to a normalized incident angle of 40°. Animations and full-resolution data products are freely available for scientific use at http://merced.gis.ucla.edu/scatterometer/index.htm.

Contents

Introduction

Since the first European Remote Sensing (ERS) satellite was launched in 1991, imaging radars have allowed observation of a wide range of natural and human-induced processes. Radars are useful in polar environments owing to their ability to penetrate clouds and the darkness of night, and their sensitivity to the presence of liquid water. Synthetic aperture radar (SAR) offers the particular advantage of high spatial resolution (~25 m for ERS). In the past decade, SAR data from the ERS, JERS, and RADARSAT satellites have been used with good results to observe ice, glacier, ocean, and land surface processes in the cryosphere.

In addition to a SAR, each ERS satellite also carries a wind scatterometer as part of its Active Microwave Instrument (AMI). The primary objective of wind scatterometers is to measure radar backscattering from ocean surface waves, from which wind velocity and direction can be estimated. However, scatterometers also collect data over land as well. Like the ERS SAR instruments, the ERS wind scatterometers operate at C-band (5.3 GHz) and VV polarization (vertically sent and received radar pulses). However, they operate over a much greater range of incident angle (18–57° as opposed to 23° for ERS SAR), have a wider illuminated swath width (500 km as opposed to 100 km), much coarser resolution (50 km, with a processed pixel spacing of 25 km), and more frequent coverage (near-daily at Arctic latitudes as opposed to 35 days for ERS SAR). Wind scatterometers therefore allow frequent radar imaging over large areas, but with coarser spatial resolution than can be achieved with SAR.

Although the primary purpose of the ERS scatterometers is to derive ocean products, their frequent global coverage allows investigation of temporally changing soil, vegetation, snow, and ice characteristics at regional to continental scales. ERS scatterometer data have now been successfully used to investigate soil freeze–thaw cycles (Boehnke and Wismann 1997; Running and others 1999; Smith and others 2000; Wismann 2000a), snow cover (Wismann and Boehnke 1997; Jin and Zhang 1999), land cover (Abdel-Messeh and Quegan 2000; Woodhouse and Hoekman 2000), sea ice (Gohin and Cavanié 1994; Cavanié 1998; Drinkwater and others 1998; Gohin and others 1998; Grandell 1998; Ezraty and Cavanié 1999; Grandell and others 1999), and the backscattering properties of the Greenland and Antarctic ice sheets (for example, Wismann 1998; Jin and Zhang 1999; Bingham and Drinkwater 2000; Drinkwater and Liu 2000; Wismann 2000b). Such scatterometer-based studies are less numerous than those using SAR. One reason for this is that scatterometer analyses require data compilation from thousands of orbits for temporal studies at the regional to continental scale. Free and easy access to user-friendly data compilations should serve a broader community of users and facilitate new research applications in Arctic and sub-Arctic environments. The Centre d'Archivage et de Traitment de données satellite released a backscatter product of ERS polar sea-ice grids (Gohin and Maroni 1998), and provides public access to these data (http://www.ifremer.fr/cersat/). This product normally provides complete spatial coverage of the polar regions, with a temporal resolution of one week or one month.

This paper presents a compilation of high temporal resolution image products with all radar backscatter data north of 60°N collected by the ERS wind scatterometers between August 1991 and December 2000. Satellite and instrument characteristics are summarized, followed by a description of the data processing procedure and instructions for download of the derived data products. Full resolution products and web-based animations are freely available for scientific use from the Department of Geography, University of California, Los Angeles.

The ERS program

The ERS satellites were launched by the European Space Agency (ESA) in July 1991 (ERS-1) and April 1995 (ERS-2). Both satellites have a Sun-synchronous near-polar orbit, with an inclination of 98° and mean altitude of 780 km. Descending orbits cross the Equator around 10:30 AM local time (ESA 1993). Wind scatterometer data were obtained from ERS-1 from 1991 to 1996. Measurements since March 1996 have been obtained from ERS-2. The wind scatterometers measure radar backscattering coefficients (σ^0) from three directions, looking 45° (forebeam), 90° (midbeam), and 135° (aftbeam) to the right of the spacecraft flight direction. ERS scatterometer data and derived wind products are distributed by IFREMER (Institut Français de Recherche pour l'Exploitation de la Mer) in the form of wind field (WNF) CD-ROM products.

Data processing procedure

ERS wind scatterometer data from IFREMER were separated into time intervals of one, three, and seven days to produce one-day, three-day, and seven-day temporal composites of radar backscatter. The one-day product offers maximum temporal resolution but suffers from spatial data gaps. The seven-day product offers reduced temporal precision but more complete spatial coverage. All three products have a grid cell spacing of 25 km, are in the polar stereographic map projection, and cover latitudes northwards from 60°N. Data products begin 1 January and end 31 December for each year except 1991 (the first year of operation for ERS-1), which begins 5 August 1991. Data processing was carried out with C and IDL (Interactive Data Language) programs written to (1) subset WNF global source data northwards from 60° latitude; (2) compile all acquired backscatter data into a grid with 25-km spacing; and (3) for each grid cell, derive a normalized radar backscatter (σ^0_{40}) that corrects for incident angle effects. Each of these three steps is described.

WNF global source data subset

Orbit swaths of raw backscatter data were extracted and subset from the global WNF source data set. Each WNF CD-ROM contains approximately three or four weeks of data organized by orbit. Each orbit contains the azimuth, incident angles, and backscatter coefficients of the fore-, mid- and aft-beams for each measurement, as well as associated sampling times and latitude/longitude coordinates. All backscatter coefficients north of 60°N were subset from the global orbit data. Concatenation of source files was commonly required to allow correct data sampling for the three-day and seven-day data products.

Compilation of backscatter data into a 25-km grid

A polar stereographic grid with 25 km cell spacing was generated for 60–90°N latitude. For each one-, three-, or seven-day time interval, all σ^0 values falling within each 25-km grid cell were compiled, and their latitude/longitude coordinates were converted to projection coordinates.

Correction for incident angle

ERS scatterometers measure the backscatter σ^0 at different incident angles for a given location on the ground, owing to a systematic increase in look angle across the image swath; the use of fore-, mid-, and aft-beams; and the fact that the satellites often return to image the same place from an adjacent orbit. Satellite measurements of σ^0 should be corrected for this effect before real changes in surface scattering properties are elucidated. In practice, this correction may be accomplished using a signal linearization method (for example, Kennett and Li 1989), which determines a linear dependence of σ^0 upon incident angle. For each 25-km grid cell, the authors determined this dependence by least-squares fit through all values of σ^0 and incident angle acquired during a specified time interval. The fit was then used to compute the σ^0 value expected for an incident angle of 40°. This corrected backscatter value (σ^0_{40}) was assigned to the cell location. Assumption of isotropic scattering is implicit in this procedure. In most cases, the least-squares regression was satisfactory for predicting fall-off of σ^0 with incident angle when data from multiple look directions were included in the regression calculation for each grid cell. Therefore, the derived least-squares relationship is assumed insensitive to sensor look direction and target orientation.

Product format and examples

All three products are in generic binary format and display σ^0_{40} in units of decibels (dB). The files within each product have a naming convention of '*mmddyyyy-MMDDYYYY*.flt,' where *mm*, *dd*, *yyyy*, *MM*, *DD*, and *YYYY* are the starting and ending day, month, and year, respectively. If the date difference is six, the file is a seven-day product. For example, the file name '01011999-01071999.flt' indicates a seven-day product from 00h00 (Universal Time Coordinate) 1 January 1999 to 24h00 7 January 1999, whereas '01011999-01011999.flt' is a one-day product for the day 1 January 1999 from 00h00 to 24h00. Most programming languages (for example, C, Fortran), image-processing and GIS systems (for example, Erdas®, ENVI®, PCI®, ER Mapper, Arc/Info®, and ArcView®), and scientific language packages (for example, IDL®, Matlab®) can read this format as a signed 32-bit float array with 273 rows and 273 columns. The center of the array, that is, cell (137, 137) corresponds to the North Pole. Latitude/longitude coordinates of cell (273, 137) are (60°N, 0°). Most backscatter data are within the range of –30 to 0 dB. A null value of zero was set for the background and missing data. No other filtering (that is, to fill data gaps) was applied.

Monthly examples of the seven-day product for year 1999 are shown in Figure 1. Variations in σ^0_{40} reflect

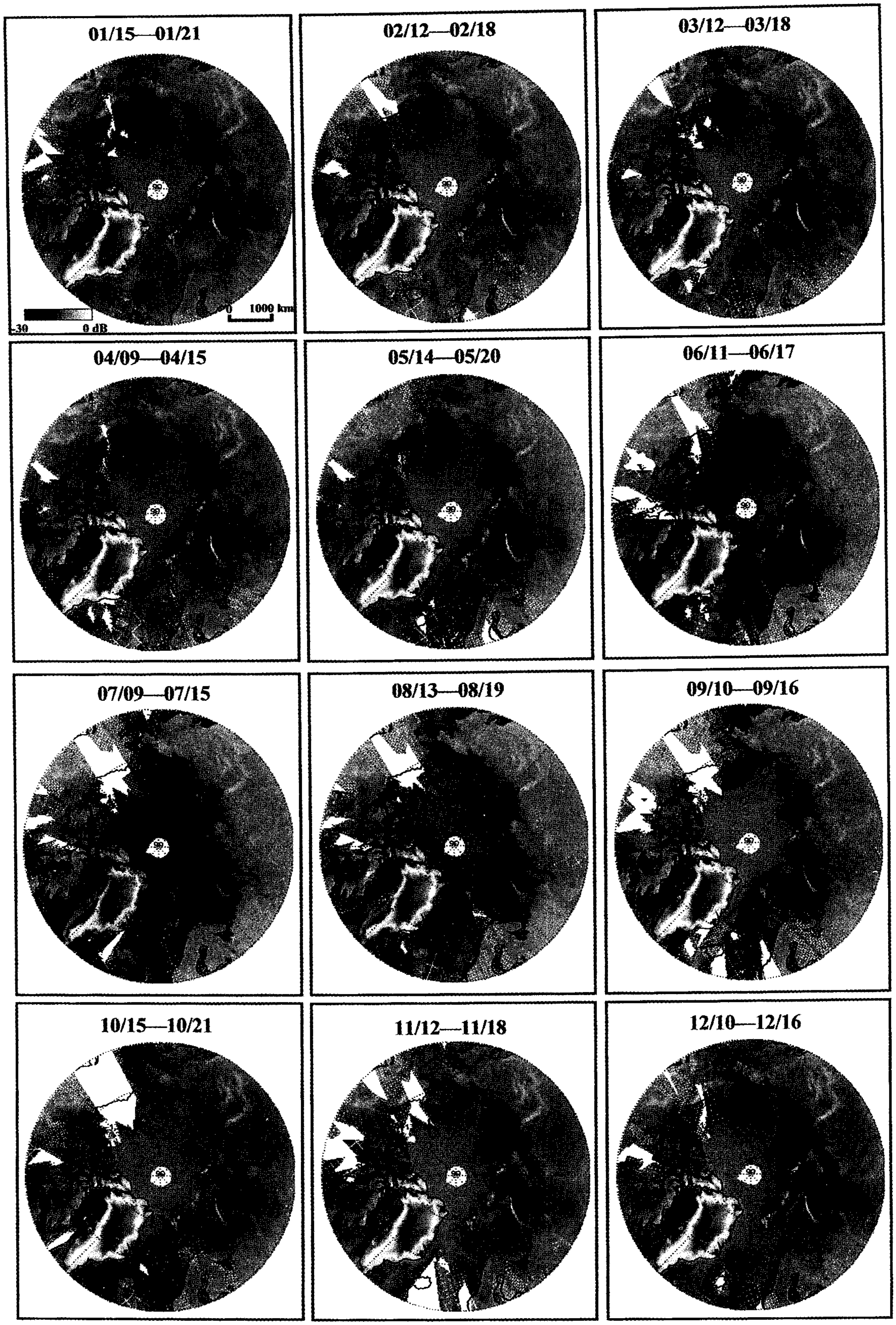

Fig. 1. Samples of the seven-day radar backscatter (σ^0_{40}) product for year 1999. Note that these images are degraded; the actual spatial resolution of all data products is 25 km. Data gaps occur where orbits are missing and northwards of 87°N. Sources of high backscattering include multi-year sea ice, percolation ice facies (Greenland), enhanced scattering by vegetation, and high topographic relief. Low backscatter is found over open water, first-year sea ice, soil thaw, and melt onset of melt over snow and ice.

dynamic changes on land, ocean, and ice surfaces. High radar returns are associated with multi-year sea ice, percolation ice facies on the Greenland ice sheet, increased soil moisture, and enhanced scattering by vegetation. Static areas of high backscatter typically correspond to areas of high topographic relief. Low values of σ^0_{40} are found over open water, first-year sea ice, thawed soils, and areas of freshly melting snow. The data gap north of 87°N apparently is caused by the orbit inclination of the ERS satellites. Smaller gaps are caused by missing orbits. Time series of backscatter can be extracted from these image products. Figure 2 shows the daily σ^0_{40} profile from 5 August 1991 to 31 December 2000 for a single 25 km pixel on the Vetrenyy ice cap (63.53°E, 80.78°N) in Zemlya Frantsa-Iosifa. Sharp decreases in σ^0_{40} correspond to the onset of melt each spring. Construction of such time series allows precise determination of the timing of melt, as well as annual and inter-annual variability in other radar backscattering properties.

Access to animations and full-resolution data products

Animations and full-resolution versions of the one-day, three-day, and seven-day data products currently span the period August 1991 to December 2000 and are freely available for scientific use at http://merced.gis.ucla.edu/scatterometer/index.htm. This article should be cited as the reference source for all animations and data downloaded from this site.

Acknowledgements

Funding for this work was provided by the National Science Foundation, through the Russian-American Initiative on Shelf-Land Environments in the Arctic (RAISE) of the Arctic System Science program (grant OPP-9818496). Wind scatterometer data were acquired by the European Space Agency and distributed by IFREMER (Institut Français de Recherche pour l'Exploitation de la Mer), Plouzané, France.

References

Abdel-Messeh, M., and S. Quegan. 2000. Variability in ERS scatterometer measurements over land. *IEEE Transactions on Geoscience and Remote Sensing* 38 (4): 1767–1776.

Bingham, A.W., and M.R. Drinkwater. 2000. Recent changes in the microwave scattering properties of the Antarctic ice sheet. *IEEE Transactions on Geoscience and Remote Sensing* 38 (4): 1810–1820.

Boehnke, K., and V. Wismann. 1997. Detecting soil thawing in Siberia with ERS scatterometer and SAR. In: *Third ERS symposium on space at the service of our environment, Florence, Italy, 14–21 March 1997.* Noordwijk: European Space Agency (ESA Special Publication 414): 35–40.

Cavanié, A. 1998. An empirical C-band backscatter melt over Arctic sea ice from ERS-1 AMI-wind data. In: *Proceedings of a joint ESA-Eumetstat workshop on emerging scatterometer applications: from research to operations, 5–7 October 1998, ESTEC, Noordwijk, The Netherlands.* Noordwijk: ESA-Eumestat (ESA Special Publication 424): 99–106.

Drinkwater, M.R., P. Wadhams, D. Low, and X. Liu. 1998. Interannual variability in Weddell Sea ice from ERS wind scatterometer. In: *Proceedings of a joint ESA-Eumetstat workshop on emerging scatterometer applications: from research to operations, 5–7 October 1998, ESTEC, Noordwijk, The Netherlands.* Noordwijk: ESA-Eumestat (ESA Special Publication 424): 119–123.

Drinkwater, M.R., and X. Liu. 2000. Seasonal to interannual variability in Antarctic sea-ice surface melt. *IEEE Transactions on Geoscience and Remote Sensing* 38 (4): 1827–1842.

ESA. 1993. *ERS-1 user handbook: revision 1.* Noordwijk: ESA Publications Division (ESA Special Publication 1148).

Ezraty R., and A. Cavanié. 1999. Intercomparison of backscatter maps over Arctic sea ice from NSCAT and ERS scatterometer. *Journal of Geophysical Research* 104 (C5): 11471–11483.

Gohin, F., and A. Cavanié. 1994. A first try at identification of sea ice using the three beam scatterometer of ERS-1. *International Journal of Remote Sensing* 15 (6): 1221–1228.

Gohin, F., A. Cavanié, and R. Ezraty. 1998. Evolution of passive and active microwave signatures of a large sea ice feature during its two and half year drift through the Arctic Ocean. *Journal of Geophysical Research* 103 (C4): 8177–8189.

Gohin, F., and C. Maroni. 1998. *Scattermeter polar ice grids user manual.* Plouzané: IFREMER/CERSAT (Technical Report C2-MUT-W-03-IF version 2.0).

Grandell, J. 1998. Possibilities for a synergetic use of coarse resolution active and passive microwaves for sea ice retrievals. In: *Proceedings of a joint ESA-Eumetstat workshop on emerging scatterometer applications: from research to operations, 5–7 October 1998, ESTEC, Noordwijk, The Netherlands.* Noordwijk: ESA-Eumestat (ESA Special Publication 424): 107–113.

Grandell, J., J.A. Johannessen, and M.T. Hallikainen. 1999. Development of a synergetic sea ice retrieval method for the ERS-1 AMI wind scatterometer and SSM/I radiometer. *IEEE Transactions on Geoscience and Remote Sensing* 37 (2): 668–679.

Jin, Y.Q., and N.X. Zhang. 1999. Correlation of the ERS and SSM/I observations over snowpack and numerical simulation. *International Journal of Remote Sensing* 20 (15–16): 3009–3018.

Kennett, R., and F. Li. 1989. SEASAT over-land scatterometer data, part I: global overview of the Ku-band backscatter coefficients. *IEEE Transactions on Geoscience and Remote Sensing* 27 (5): 592–605.

Running, S.W., J.B. Way, K.C. McDonald, J.S. Kimball, S. Frolking, A.R. Keyser, and R. Zimmerman. 1999. Radar remote sensing proposed for monitoring freeze–thaw transitions in boreal regions. *EOS, Transactions, American Geophysical Union* 80 (213): 220–221.

Smith, L.C., G.A. MacDonald, K.E. Frey, A. Velichko, K. Kremenetski, O. Borisova, and R.R. Forster. 2000. US-Russia venture probes Siberian peatlands' sensitivity to climate. *EOS, Transactions, American Geophysical Union* 81 (491): 503–504.

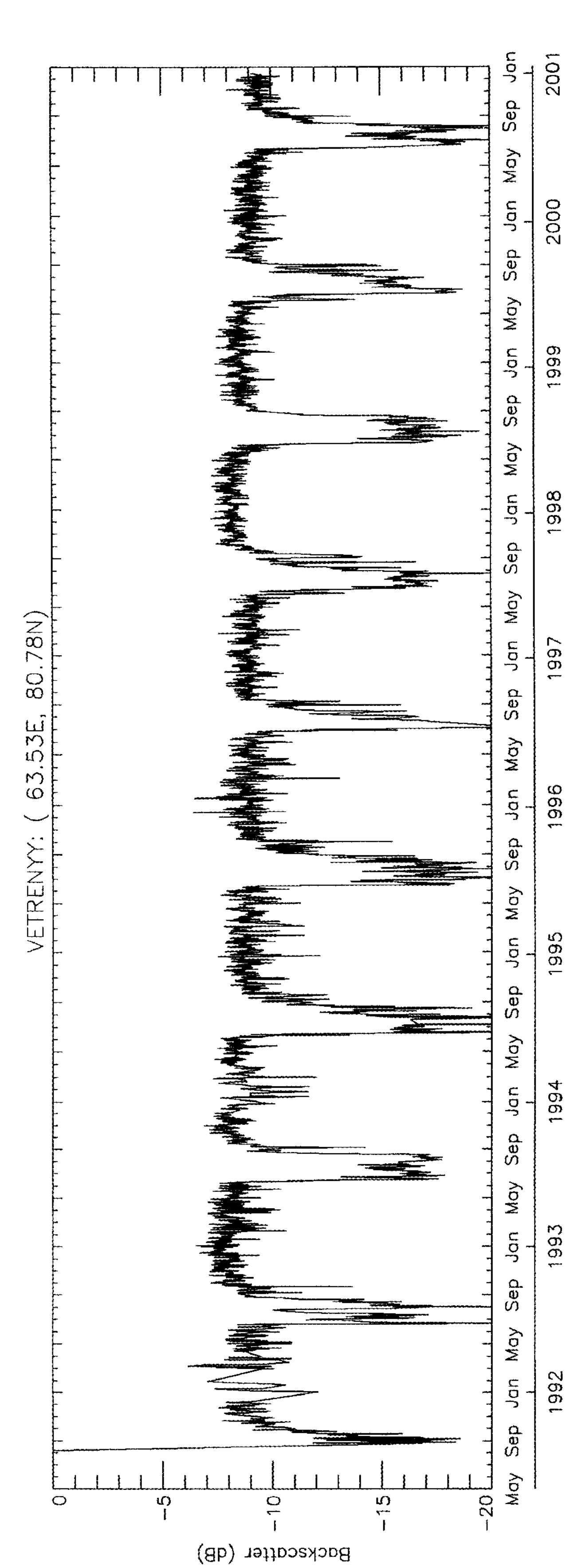

Fig. 2. Daily radar backscatter time series extracted from one-day σ^0_{40} data product for a single pixel (63.53°E, 80.78°N) on the Vetrenyy ice cap, Zemlya Frantsa-Iosifa. Sharp decreases in σ^0_{40} are associated with the annual onset of melt.

Wismann, V. 1998. Land surface monitoring with spaceborne scatterometers. In: *Proceedings of a joint ESA-Eumetstat workshop on emerging scatterometer applications: from research to operations, 5–7 October 1998, ESTEC, Noordwijk, The Netherlands.* Noordwijk: ESA-Eumestat (ESA Special Publication 424): 25–31.

Wismann, V. 2000a. Monitoring of seasonal thawing in Siberia with ERS scatterometer data. *IEEE Transactions on Geoscience and Remote Sensing* 38 (4): 1804–1809.

Wismann, V. 2000b. Monitoring of seasonal snowmelt on Greenland with ERS scatterometer data. *IEEE Transactions on Geoscience and Remote Sensing* 38 (4): 1821–1826.

Wismann, V., and K. Boehnke. 1997. Monitoring snow properties on Greenland with ERS scatterometer and SAR. In: *Third ERS symposium on space at the service of our environment, Florence, Italy, 14–21 March 1997.* Noordwijk: European Space Agency (ESA Special Publication 414): 857–861.

Woodhouse, I.H., and D.H. Hoekman. 2000. Determining land-surface parameters from the ERS wind scatterometer. *IEEE Transactions on Geoscience and Remote Sensing* 38 (1): 126–140.